



Inhibition of DOT1L and PRMT5 promote synergistic anti-tumor activity in a human *MLL* leukemia model induced by CRISPR/Cas9

Kathy-Ann Secker¹ · Hildegard Keppeler¹ · Silke Duerr-Stoerzer¹ · Hannes Schmid¹ · Dominik Schneidawind¹ · Thomas Hentrich² · Julia M. Schulze-Hentrich² · Barbara Mankel³ · Falko Fend³ · Corina Schneidawind¹

Received: 4 October 2018 / Revised: 30 April 2019 / Accepted: 29 May 2019 / Published online: 15 August 2019
© The Author(s), under exclusive licence to Springer Nature Limited 2019

Abstract

MLL rearrangements play a crucial role in leukemogenesis and comprise a poor prognosis. Therefore, new treatment strategies are urgently needed. We used the CRISPR/Cas9 system to generate an innovative leukemia model based on 100% pure *MLL-AF4* or *-AF9* rearranged cells derived from umbilical cord blood with indefinite growth in cell culture systems. Our model shared phenotypical, morphological and molecular features of patient cells faithfully mimicking the nature of the disease. Thus, it serves as a fundamental basis for pharmacological studies: inhibition of histone methyltransferase disruptor of telomeric silencing 1-like (DOT1L) is one specific therapeutic approach currently tested in clinical trials. However, success was limited by restricted response warranting further investigation of drug combinations. Recently, it has been shown that the inhibition of protein arginine methyltransferase 5 (PRMT5) exhibits anti-tumoral activity against human cell lines and in *MLL* mouse models. Here, we used DOT1L and PRMT5 inhibitors in our human *MLL*-rearranged model demonstrating dose-dependent reduced proliferation, impairment of cell cycle, increasing differentiation, apoptosis, downregulation of target genes and sensitization to chemotherapy. Strikingly, the combination of both compounds led to synergistic anti-tumoral effects. Our study provides a strong rationale for novel targeted combination therapies to improve the outcome of *MLL*-rearranged leukemias.

Introduction

The *MLL/KMT2A* gene is frequently translocated in acute leukemias leading to an epigenetic dysregulation responsible for the oncogenic properties of the disease [1]. *MLL*-rearranged (*MLLr*) leukemias account for over 80% in infants and about 10% in adults [2]. The prognosis is dismal

and current therapeutic approaches are accompanied with several severe side effects induced by intensive chemotherapy regimens employed with only limited success [3]. Thus, new targeted therapeutic strategies are urgently needed to improve the outcome of these patients. The impact of *MLL* fusion proteins on the pathogenesis of the disease has already been investigated in various mouse models using retrovirally overexpressed *MLL* oncogenes, which commonly lead to incommensurable results for the underlying patient disease [4–9]. Therefore, representative human models to test new compounds are urgently required, since primary leukemic cells are not suitable due to their limitation of rapid differentiation in in vitro cultures. Recently, we and others utilized novel genetic tools for genome editing in primary human hematopoietic stem and progenitor cells (HSPCs) with intent to generate a new representative *MLL* leukemia model [10–15]. We were able to generate *MLL-AF9* cells with transcription activator-like effector nucleases (TALENs) showing indefinite monoclonal outgrowth in in vitro cultures by using a cytokine milieu based on the requirements of rearranged cells [11]. Although this approach recapitulated many features of the

Supplementary information The online version of this article (<https://doi.org/10.1038/s41388-019-0937-9>) contains supplementary material, which is available to authorized users.

✉ Corina Schneidawind
corina.schneidawind@med.uni-tuebingen.de

- ¹ Department of Hematology and Oncology, University Hospital Tuebingen, Tuebingen, Germany
- ² Institute of Medical Genetics and Applied Genomics, University of Tuebingen, Tuebingen, Germany
- ³ Institute of Pathology and Neuropathology, University of Tuebingen and Comprehensive Cancer Center, University Hospital Tuebingen, Tuebingen, Germany

disease, the results were limited due to technical issues based on extensive in vitro cultures to obtain sufficient numbers of translocated cells for further investigations [11]. In this report, we used the clustered regularly interspaced short palindromic repeats (CRISPR)/Cas9 system with high efficiency to specifically engineer reciprocal chromosomal translocations in primary human HSPCs not only in the *MLL* and *AF9* genes, but also in the *AF4* gene representing the first reliable human *MLL-AF4* model based on patient sequences.

AF4 and *AF9* account for the majority in over 100 different known fusion partners of the *MLL* gene [2]. The resultant fusion proteins arouse their oncogenic properties by recruiting cofactors like the H3K79 methyltransferase DOT1-like (DOT1L) serving as ideal target for new therapeutic strategies [16]. Although DOT1L inhibition has an acceptable side effect profile (clinical trial NCT01684150), it shows only modest clinical activity in adult leukemias and further combination approaches are required to improve efficiency [17]. *Protein arginine methyltransferase 5 (PRMT5)* is known to be overexpressed in several solid tumors and correlates with a poor prognosis [18, 19]. Thus, one clinical trial has already been implemented to test small molecules that inhibit PRMT5 in patients with relapsed solid tumors or non-Hodgkin's lymphoma (NCT02783300). Recently, Kaushik et al. and Serio et al. also highlighted the impact for PRMT5 inhibition in mouse models of *MLLr* leukemia in vivo and in human *MLLr* cell lines in vitro but until now no human *MLL* model exists demonstrating the anti-tumoral activity of this compound [20, 21]. We administered inhibitors of DOT1L and PRMT5 in our *MLL* leukemia model resulting in anti-leukemic effects that were significantly enhanced when both drugs were applied simultaneously. Both compounds conveyed these effects without any negative impact on control cells. Remarkably, addition of both compounds to standard chemotherapy either as pretreatment or co-administered simultaneously improved *MLLr* cell killing. Our model can overcome existing limitations in genome editing techniques and pharmacological studies allowing to reliably test new targeted therapies. We thereby establish the preclinical rationale to target PRMT5 and DOT1L in the treatment of leukemia patients harboring *MLL* translocations.

Results

CRISPR/Cas9 demonstrates high cutting efficiencies and induces *t(9;11)* and *t(4;11)* chromosomal translocations in human HSPCs

Previous studies have identified frequent *MLL-AF4* and *-AF9* chromosomal translocation breakpoints in patients [2]. Using CRISPRscan, we designed different sgRNAs

recognizing patient-specific sequences in intron 11 of the *MLL*, exon 3 of the *AF4* and intron 5 of the *AF9* genes, respectively [4, 22, 23]. Using plasmid- and virus-free delivery of sgRNAs with Cas9 protein, we nucleofected K562 cell line as proof-of-principle to identify the best working sgRNAs for the respective regions. Following nucleofection genomic DNA was isolated and the targeted regions of interest were amplified via PCR and analyzed by the T7 endonuclease I assay showing high cutting efficiencies (Fig. 1a, upper row) [24]. The sgRNAs most efficient at cleavage were further validated in our CD34⁺ target cells derived from human umbilical cord blood (huCB) (Fig. 1a, lower row). To induce *t(9;11)* and *t(4;11)* translocations in HSPCs, we isolated CD34⁺ cells and nucleofected with Cas9 protein and sgRNAs targeting *MLL* and *AF4* or *AF9*, respectively. Cas9 alone was used as control. Following nucleofection, *MLL-AF4* and *-AF9* fusion junctions were detected by PCR and Sanger sequencing demonstrating specific fusion sequences (Fig. 1b, c and Supplementary Fig. 1a).

Engineered *MLLr* cells rapidly reach purity, express fusion transcripts and present with a myelomonocytic phenotype

Following nucleofection, the cells were maintained in liquid culture supplemented with cytokines and chemokines optimized for growth of *MLLr* cells [11]. PCR analyses of genomic DNA showed increasing signals from *MLL-AF4*, *MLL-AF9* and the respective reciprocal fusion junctions over time (Fig. 2a and Supplementary Fig. 1b). To quantify the percentage of cells with translocations, FISH analysis was performed. On day 30 (*MLL-AF4*) and day 40 (*MLL-AF9*) of liquid culture, an *MLL* break-apart probe detected *MLL* translocations in 100% of cells allowing for further analysis of pure *MLLr* cells (Fig. 2b). Likewise, G-banding analysis demonstrated the presence of both derivative chromosomes resulting in reciprocal *t(4;11)* and *t(9;11)* translocations (Fig. 2c). To confirm the functional expression on RNA level RT-PCR analyses were performed revealing both *MLL-AF4* and *-AF9* fusion transcripts (Fig. 2d, Supplementary Fig. 1c and Supplementary Table 4).

Patients harboring *MLL* translocations typically present myelomonocytic surface markers and loss of CD34 expression on their blast cells [25, 26]. Similarly, the genome-engineered *MLLr* cells in our model displayed a myelomonocytic phenotype with CD64 and CD15 and low expression of CD34 and CD38, respectively (Fig. 2e). Interestingly, the *MLLr* cells express less mature markers like CD14 and presented with *MLLr* typical leukemic surface expressions of CD9 and CD32 compared with control cells as recently published (Fig. 2f) [11, 25]. These results demonstrate that using CRISPR/Cas9 targeting *MLL* and *AF4/AF9* creates

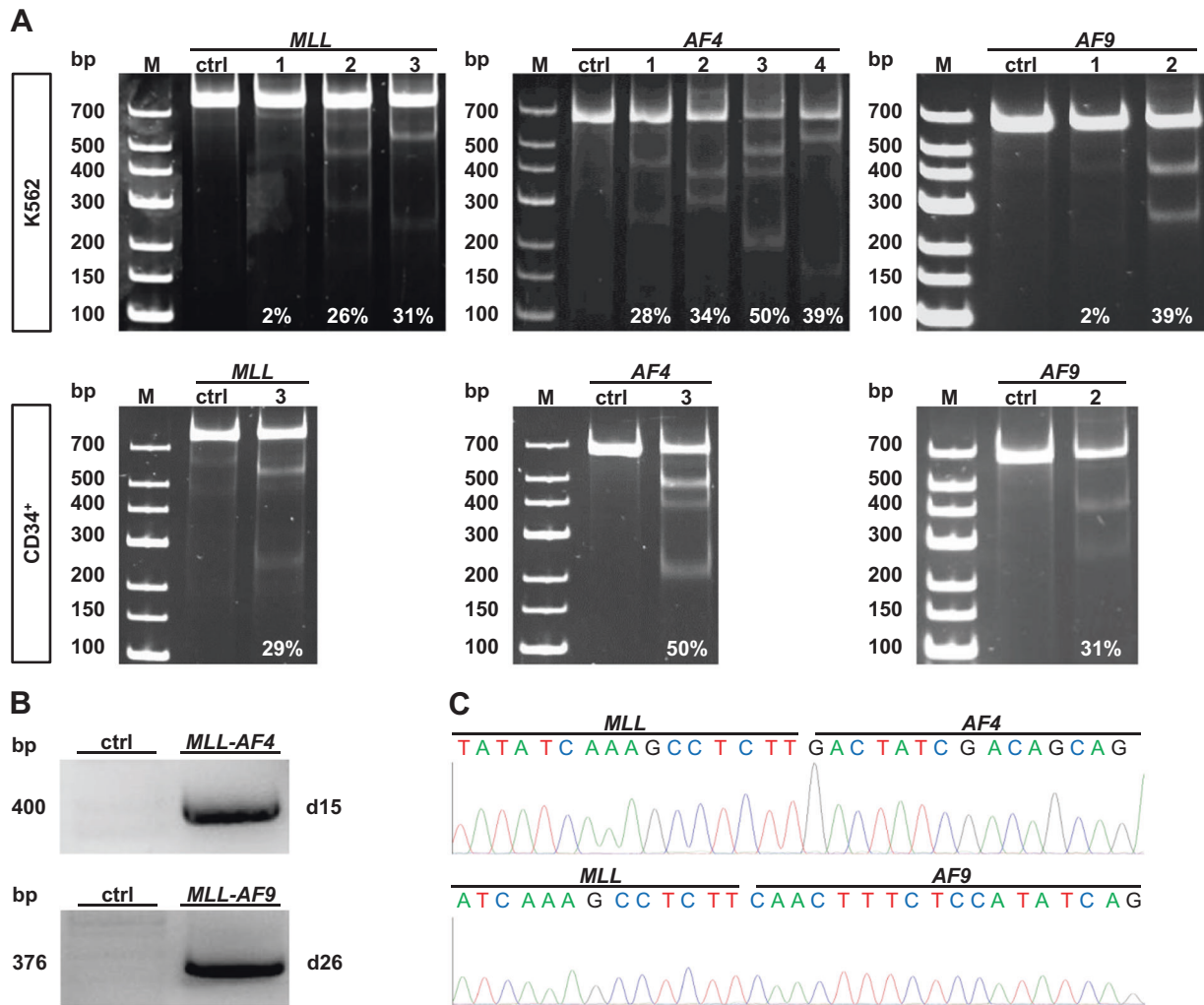


Fig. 1 CRISPR/Cas9 induces specific double-strand DNA breaks within the *MLL*, *AF4*, and *AF9* genes leading to translocations in HSPCs. **a** Gel images show representative results of T7 endonuclease assays performed on genomic DNA isolated from K562 cells (upper row) nucleofected with the different sgRNAs (*MLL*: 1–3, *AF4*: 1–4, *AF9*: 1–2) and Cas9 protein. The sgRNAs with the best cutting efficiencies in K562 were applied to CD34⁺ cells (lower row). K562 cells or CD34⁺ huCB cells nucleofected with Cas9 alone were used as controls (ctrl). Digested PCR products represent the presence of strand

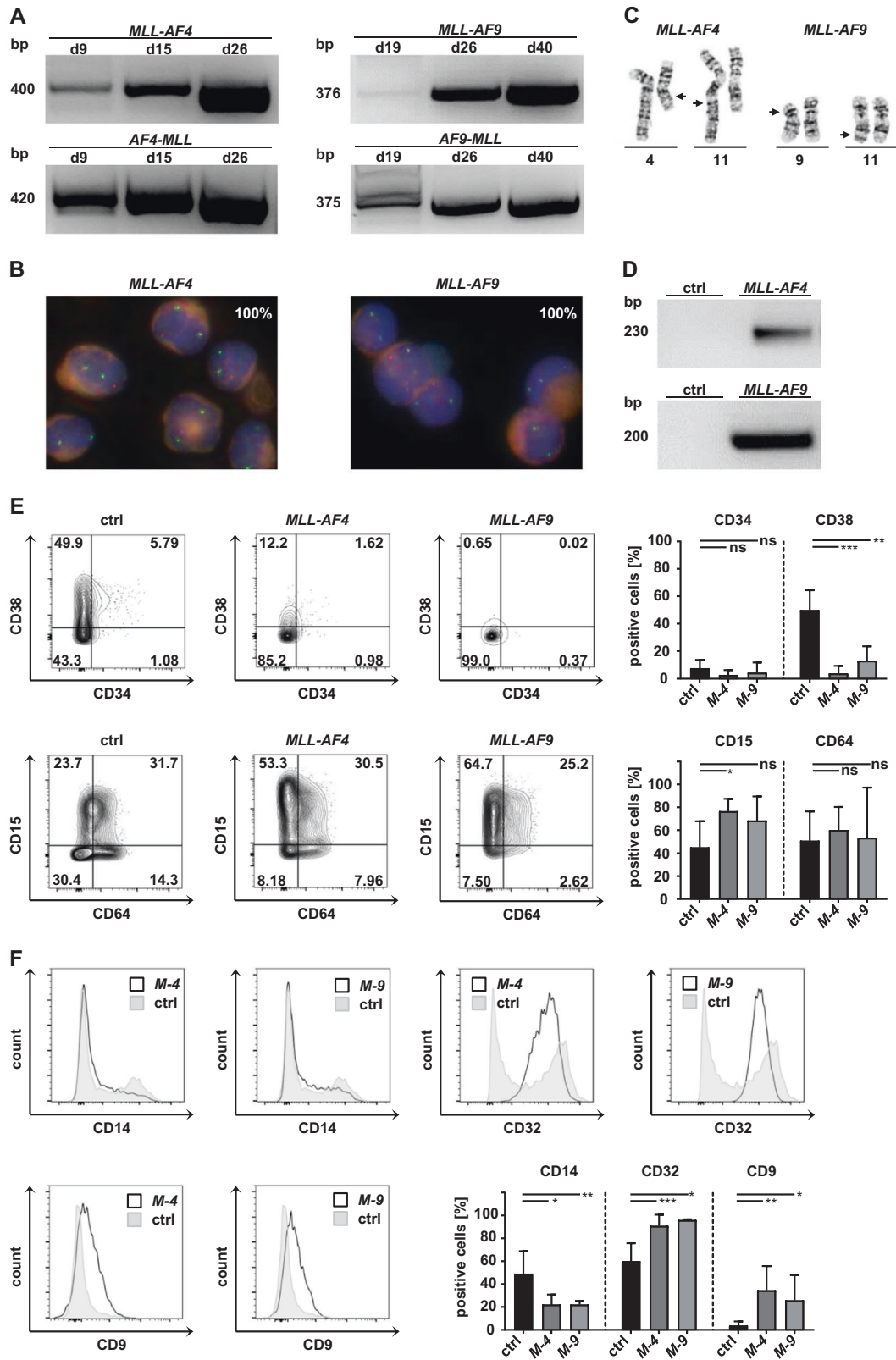
mismatches resulting from indels that are generated by non-homologous end joining (NHEJ) repair of double-strand breaks (DSBs) and were quantified with ImageJ. Resulting cutting efficiencies are displayed. **b** Representative positive PCR products of genomic DNA isolated from CD34⁺ cells nucleofected with *MLL* sgRNA3 and *AF4* sgRNA3 or *AF9* sgRNA2 and Cas9 protein or Cas9 alone as controls (ctrl) on day 15 and day 26 of culture, respectively. **c** Sanger sequencing results of PCR products displayed in **(b)** showing translocated gene products of *MLL-AF4* and *MLL-AF9*

t(9;11) and *t(4;11)* chromosomal translocations, which induce respective fusion transcript expressions and are characterized by a patient-like myelomonocytic phenotype.

RNA-seq reveals patient-like gene expression profile of *MLL-AF4* rearranged cells

To validate our *MLL*_r leukemia model as a suitable patient-like in vitro model, we compared the transcriptome of our genome-engineered and control cells to publicly available patient samples harboring an *MLL-AF4* rearrangement [27, 28]. *MLL-AF4* translocated cells and the respective

control cells from the two different donors were maintained in similar culture conditions. After reaching 100% purity of the *MLL*_r cells, they were subjected to RNA-seq. Comparing the gene expression profiles of the *MLL-AF4* cells with the respective controls, we found 2729 of the 13276 genes (~21%) to be differentially expressed ($p < 0.01$), of which 1417 were upregulated in the *MLL*_r cells (Supplementary Fig. 2a). Sample correlation revealed a higher similarity of *MLL-AF4* translocated cells between different donors than to their respective control cells (Supplementary Fig. 2b). We listed our 100 most differentially genes (50 up- and 50 downregulated) in Supplementary Table 5. Similarly, in



comparison to the top 100 genes in *MLLr* patients, we also detected *MEIS1* and *FLT3* supporting their conserved roles in the *MLL* leukemogenesis and in our model [28]. Moreover,

within this top 100 most differentially genes in *MLLr* patients, we found these five genes *MEIS1*, *APOL2*, *GFOD1*, *SPTBN1*, and *ZNF827* almost identically expressed compared

◀ **Fig. 2** Pure *MLL-AF4* and *-AF9* cells showing indefinite growth in vitro cultures and present with typical *MLLr* myelomonocytic immunophenotype. **a** Representative semi-quantitative PCR of genomic DNA (100 ng) isolated from CD34⁺ cells nucleofected with sgRNAs for *MLL*- and *AF4/AF9* over time of culture showing increasing *MLL-AF4/-AF9* and the respective reciprocal PCR products. **b** FISH analyses of CD34⁺ cells nucleofected with sgRNAs for *MLL* and *AF4* or *AF9* were performed after reaching strong PCR products (on day ~30 of culture) via manual inspection of 100 cells demonstrating 100% purity of the *MLLr* cells, and **c** representative karyotyping. Arrows indicate the reciprocal breaks. **d** mRNA was isolated from *MLL-AF4/-AF9* cells or control (ctrl; CD34⁺ cells nucleofected with Cas9 alone) and fusion transcripts were identified by RT-PCR. **e** Flow cytometry of *MLLr* cells reveals stable myelomonocytic expressions of CD15 and CD64 and low expression of CD34 and CD38 after reaching purity. Representative and combined results of three biological replicates ($n = 3$). **f** *MLLr* cells present with lower expression levels of differentiation marker CD14 and higher expression of known *MLLr* surface markers (CD32 and CD9) compared with control cells (ctrl; CD34⁺ huCB cells nucleofected with Cas9 alone and cultured for the same time) [11, 25]. Gray shading indicates control cells; black line denotes indicated marker expression of *MLLr* cells. Representative and combined results of three biological replicates ($n = 3$). *M-4*, *MLL-AF4*; *M-9*, *MLL-AF9*. Bars represent the mean. Student's *t* test was used: * $p < 0.05$, ** $p < 0.01$, *** $p < 0.001$. Error bars indicate standard deviation (SD)

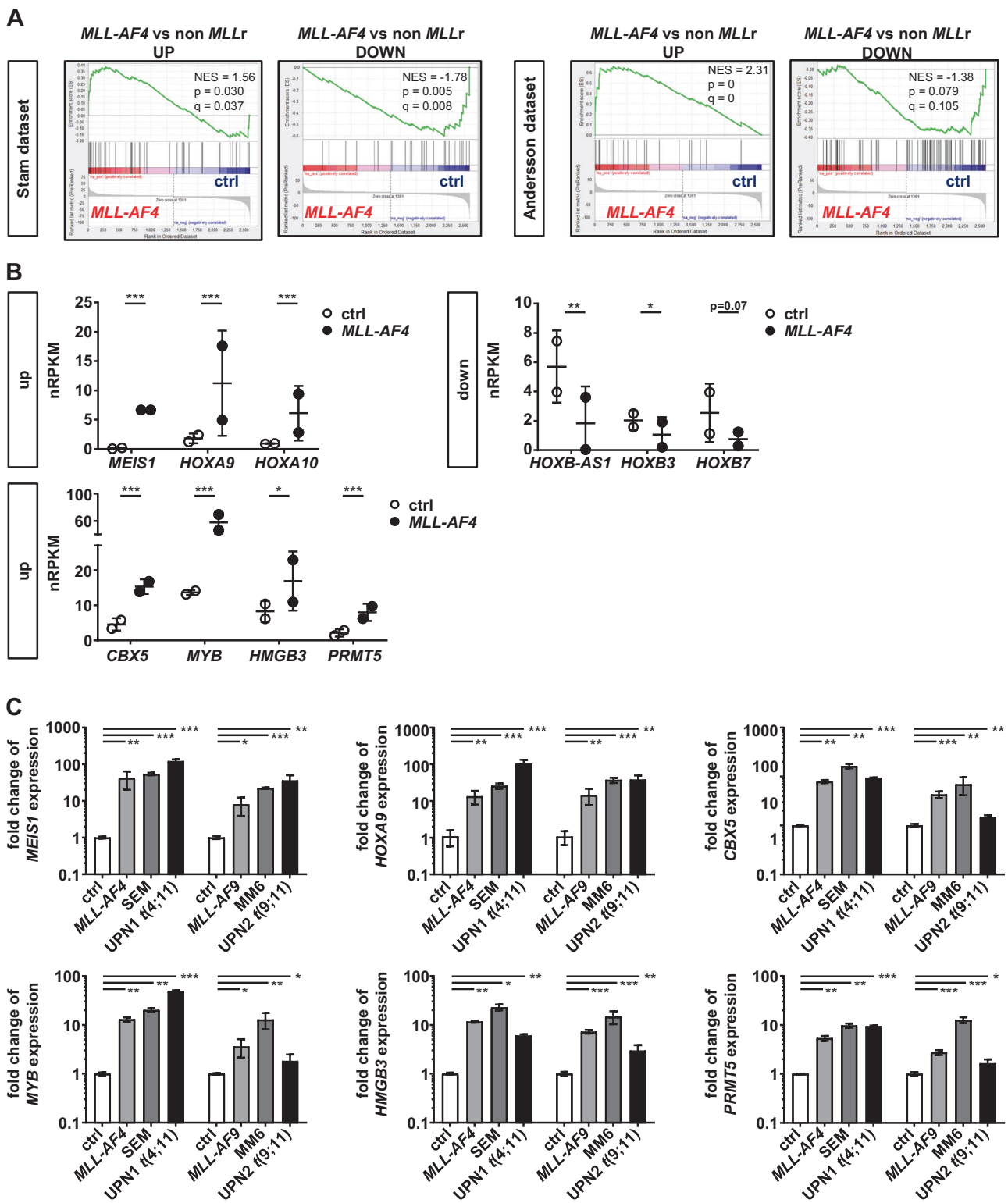
with our *MLLr* model (Supplementary Fig. 2c) [28]. To further highlight the comparability of our human in vitro model to patient *MLLr* leukemia we performed gene set enrichment analyses (GSEA), which confirmed significant enrichment of patient-derived *MLL-AF4* signatures (Fig. 3a) [27–30]. Our model demonstrated a typical *MLLr* leukemia signature, such as upregulation of *HOXA* cluster and downregulation of *HOXB* cluster (Fig. 3b) [31–33]. In addition, self-renewing leukemic stem cell (LSC) signature defined by overexpression of *CBX5*, *MYB*, and *HMGB3* was observed in our *MLL-AF4* model (Fig. 3b) [34]. Overexpression of *PRMT5* is known to correlate with poor prognosis in several tumors [18, 19]. Furthermore, *MLLr* mouse models identified *PRMT5* as one potential driver of *MLL* leukemogenesis [21, 35]. Here, we confirmed *PRMT5* overexpression in the RNA-seq data of our human patient-like system, supporting its important role to validate targeted therapy (Fig. 3b). For further confirmation of the RNA-seq data, we performed qPCR of representative target genes, LSC signature and *PRMT5*. *MLL-AF4* and *MLL-AF9* translocated cells express high levels of *MEIS1*, *HOXA9*, *CBX5*, *MYB*, *HMGB3*, and *PRMT5* comparable to the *MLL-AF4* cell line SEM, the *MLL-AF9* cell line MONO-MAC-6 (MM6) and patient leukemic cells harboring $t(4;11)(q21;q23)$ or $t(9;11)(p22;q23)$ (Fig. 3c and Supplementary Table 6).

These data indicate that the expression profile of our model correlates with *MLLr* leukemia patients therefore faithfully mimicking the nature of the underlying disease. Furthermore, our results revealed *PRMT5* to be a potentially suitable target in the treatment of poor prognosis *MLLr* leukemias.

Inhibition of both DOT1L and PRMT5 acts synergistically and restrains proliferation of *MLLr* cells

The *MLL* fusion protein gains new function through recruitment of other cofactors like DOT1L. DOT1L hereby acts as catalyst for the *MLL* fusion protein-driven transformation and accordingly, serves as specific therapeutic target in this disease [16, 36]. However, until now the efficacy of DOT1L inhibition as a single agent was only modest in clinical trials [17]. Recently, it has been demonstrated that *PRMT5* as a direct target of polymerase-associated factor complex (PAFc) interacting with the *MLL* fusion protein contributes to the progression and maintenance of *MLL*-driven leukemia in mouse models and in human cell lines in vitro [21, 35]. To study the impact of DOT1L and *PRMT5* inhibition alone and in combination, we performed a proliferation assay using our human *MLLr* model system: we monitored proliferation by cell counting with Trypan blue staining of *MLL-AF4* and *-AF9* or control cells in the presence of increasing concentrations of EPZ004777 (DOT1Li) and EPZ015666 (*PRMT5*i) for 6 days. For both inhibitors, we found a dose-dependent inhibition of *MLLr* cell proliferation whereas control cells were only affected when the highest concentration of *PRMT5*i was used (Supplementary Fig. 3a). It is known that DOT1L contributes to the transcriptional activation of target genes [16]. Therefore, following inhibition of DOT1L we determined cellular differentiation by monitoring expression of the differentiation marker CD14 via flow cytometry. As expected, we found a dose-dependent increase of CD14 expression in our DOT1Li-treated *MLLr* cells whereas control cells were not affected (Supplementary Fig. 3b). Recently, it has been demonstrated that *PRMT5* is responsible for methylating p53. Consequently, depletion of *PRMT5* triggers p53-dependent apoptosis [37]. Therefore, we determined apoptosis via Annexin V staining by flow cytometry upon *PRMT5*i treatment and confirmed a dose-dependent increase of apoptotic cells in *MLLr* cultures (Supplementary Fig. 3b). According to these results, we considered a concentration of 1 μ M for both inhibitors in further experiments. To improve therapeutic effectiveness to treat *MLLr* leukemias, we tested a combination of DOT1Li and *PRMT5*i for synergy in our *MLLr* model. For that purpose, we performed again dose response curves of single and combination treatment of both compounds at a constant ratio of equipotency (Supplementary Fig. 4a). For synergy determination, IC₅₀ values were interpolated (Supplementary Fig. 4b) and isobolograms at 50% effect level as well as the calculation of combination indexes (CI < 1) indicate synergism (Supplementary Fig. 4c).

Next, to evaluate the effect of the compounds on proliferation, we used our *MLLr* model for single and



combination treatment and determined cell count via microscopy and flow cytometry. Inhibitors alone already induced significant reduction of proliferation, whereas both compounds further enhanced the growth-inhibitory effect

(Fig. 4a, b). The anti-proliferative capacity of DOT1L and PRMT5 inhibition was also demonstrated in cell cycle analysis: BrdU and 7-AAD staining revealed no changes in control cells, whereas a decrease in the percentage of *MLLr*

◀ **Fig. 3** *MLL-AF4* rearranged cells revealed patient-like gene expression profile. RNA-seq was performed with *MLL-AF4* cells (two different donors, $n = 2$) and the respective controls (two different donors, $n = 2$, CD34⁺ huCB cells of the same donor nucleofected with Cas9 alone and cultured for the same time). **a** Gene set enrichment analysis of the *MLL-AF4* signature derived from two published patient datasets are shown: upregulated gene sets in patients (*MLL-AF4* vs non-*MLLr* UP) are enriched in *MLL-AF4* translocated cells, while downregulated gene sets in patients (*MLL-AF4* vs non-*MLLr* DOWN) are enriched in control cells of our model. Values indicate normalized enrichment score (NES), p -value for statistical significance and q -value for the false discovery rate (FDR). **b** Differential gene expression by RNA-seq of the *MLLr* cells compared with control cells examined characteristic up- and downregulation of known *MLLr* target genes plotted as individual data points with mean (upper row). Known upregulation of a leukemia stem cell signature (*CBX5*, *MYB*, and *HMGB3*) as well as overexpression of *PRMT5* are shown (lower row). Values in normalized reads per kilobase million (nRPKM), each dot represents a sample ($n = 2$). **c** Validations of target genes, *CBX5*, *MYB*, *HMGB3*, and *PRMT5* profiled by RNA-seq were confirmed by qPCR. *MLL-AF4* and *MLL-AF9* cells were normalized to control (ctrl; CD34⁺ huCB cells of respective donors nucleofected with Cas9 alone and cultured for the same time) and compared with the *MLL-AF4* cell line SEM or *MLL-AF9* cell line MM6 and patient cells (unique patient number, UPN1 and UPN2) harboring $t(4;11)(q21;q23)$ or $t(9;11)(p22;q23)$, respectively. Experiment was performed in biological duplicates ($n = 2$) and horizontal bars represent the mean. Student's t test was used: * $p < 0.05$, ** $p < 0.01$, *** $p < 0.001$. Error bars indicate SD

cells in the S phase was detected by the respective single treatment that was further enhanced by the combination of the compounds (Fig. 4c).

These data indicate that the inhibition of DOT1L and PRMT5 results in a synergistic suppression of proliferation and reduction of DNA synthesis in *MLL* fusion protein-driven leukemogenesis without impact on control cells.

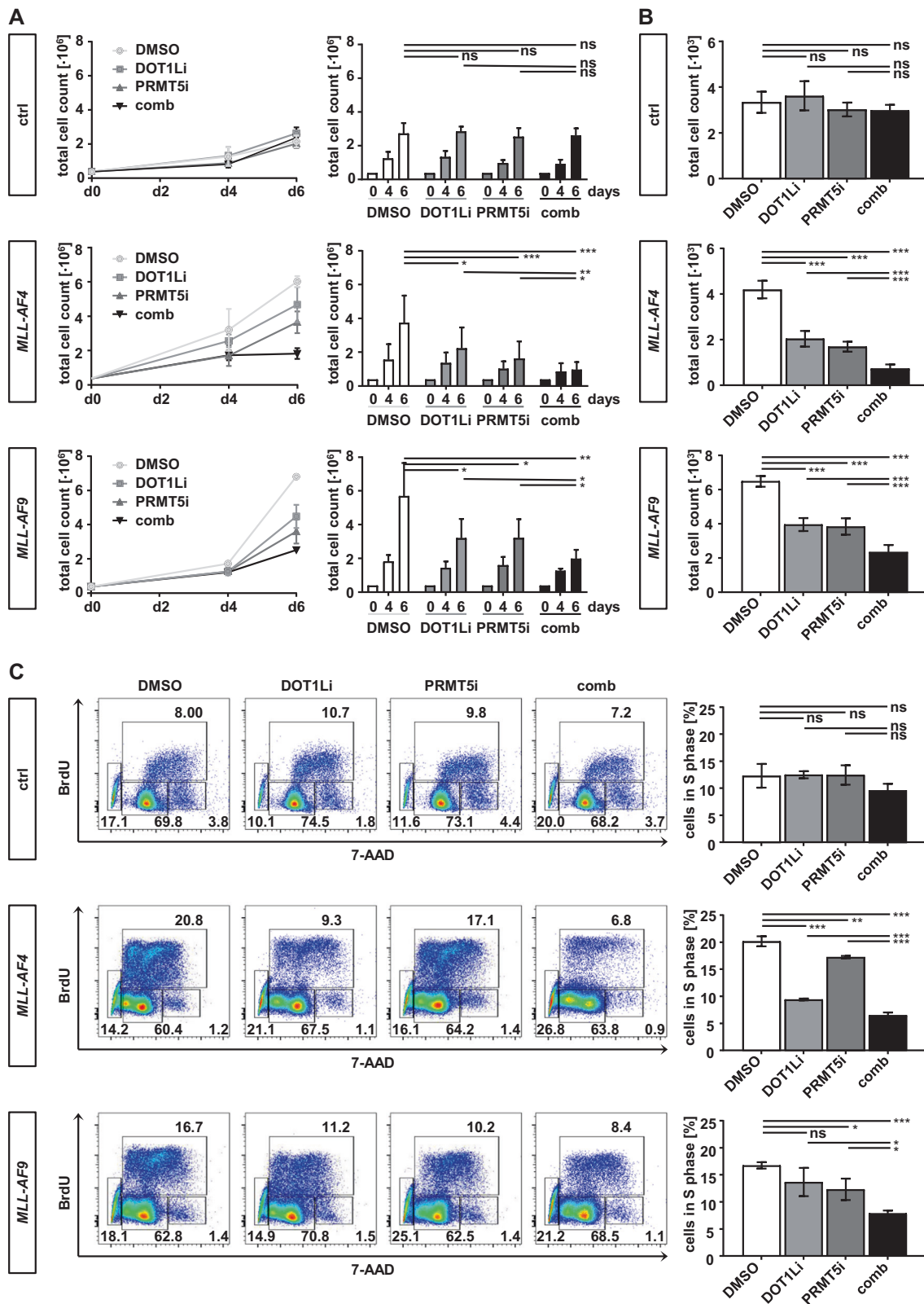
Inhibition of DOT1L and PRMT5 compromises *MLL* leukemogenesis by alternative pathways resulting in increased apoptosis of *MLLr* cells

Recently, it has been shown in an *MLL-AF9* mouse model that PRMT5i does not affect direct *MLL* target gene expression [35]. Similarly, we found downregulation of target gene expression such as *HOXA9* and *MEIS1* upon DOT1L but not PRMT5 inhibition (Fig. 5a). In contrast to PRMT5i, treatment with DOT1Li significantly promoted *MLLr* cell differentiation assessed by upregulation of CD14 consistent with our findings and those of Serio and colleagues, respectively [10, 21]. Subsequently, we performed May-Gruenwald-Giemsa staining to evaluate cell morphology after respective treatments. Untreated (DMSO control) *MLLr* cells presented an immature myelomonocytic phenotype whereas treatment with DOT1Li resulted in morphologic changes to macrophage-like cells consistent with the detected CD14 expression (Fig. 5b, c, d). In contrast, PRMT5i led to induction of apoptosis that was further pronounced in the combined treated samples (Fig. 5e).

Likewise, *MLLr* cells showed a significantly higher percentage of Annexin V positive cells when treated with both inhibitors compared with single compounds indicating that combination treatment leads to synergistic apoptosis (Fig. 5e). Importantly, key findings could be verified using alternative inhibitors against DOT1L (EPZ5676, aDOT1Li) and PRMT5 (EPZ015938, aPRMT5i) (Supplementary Fig. 5). These data suggest that DOT1L and PRMT5 contribute to *MLL*-driven leukemia in two pathways: DOT1L leads to increased transcription of target genes promoting maturation arrest and PRMT5 inhibits apoptosis. Both compounds act synergistically by inhibiting proliferation, inducing apoptosis and promoting differentiation in our human *MLLr* model.

Treatment with DOT1Li and PRMT5i sensitizes *MLLr* cells to chemotherapy

To further determine the activity of both inhibitors in a more clinical setting, we determined the fate of *MLLr* cells after removal of the compounds and the impact of combining the inhibitors with chemotherapy on proliferation and cell cycle of *MLLr* cells. For that purpose, we treated the cells with the compounds alone or in combination for 6 days, washed the compounds out, reseeded the cells at the same concentration and subsequently determined cell count and cell cycle. Although treatment of *MLLr* cells stopped, proliferation was still significantly reduced indicated by the low cell count and enhanced doubling time (T_d) compared with untreated *MLLr* cells (Supplementary Fig. 6a, b). The reduced cell growth was most pronounced by the preceding combination treatment, implying a durable reprogramming of the epigenetic status of these cells after inhibitory treatment. As expected, the compounds induced both apoptosis and reduced DNA synthesis, that was only partially rescued after 4 days of interrupted treatment. Interestingly, the compounds did not influence G0/G1 phase of the treated *MLLr* cells (Supplementary Fig. 6c) implying that both compounds may not impede chemotherapy responses. Cytarabine represents one of the most commonly used chemotherapy agents to treat patients with AML. Therefore, we evaluated the effect of DOT1Li and PRMT5i on the proliferation of the *MLLr* cells when used in combination with cytarabine either simultaneously or sequentially with compound-pretreated cells. First, we titrated cytarabine alone and in combination with the compounds and determined 5 nM as an appropriate concentration to evaluate potential additional effects in our *MLLr* model (Fig. 6a). Co-administration of cytarabine with the respective inhibitors simultaneously induced a superior effect on the *MLLr* cell killing than cytarabine alone, which was again increased by using both compounds at once (Fig. 6b). For the sequential treatment experiments, we pretreated *MLLr* cells with the



respective inhibitors again for 6 days, washed them out and added cytarabine to the culture for another 2 days. Remarkably, also in the sequential treatment we can observe the complementary effect of the compounds on

chemotherapy response, indicating that the preceding epigenetic alteration sensitizes them to chemotherapeutic agents, even when the inhibitors have been removed (Fig. 6c). Taken together, our results showed that both PRMT5i and

◀ **Fig. 4** Inhibition of both DOT1L and PRMT5 acts synergistically and inhibits proliferation in *MLLr* cells. *MLL-AF4-AF9* or culture-expanded CD34⁺ huCB control cells were treated with either 1 μM DOT1Li, 1 μM PRMT5i, in combination or vehicle (DMSO) for 6 days. **a** To demonstrate proliferation curves, total cell count was determined by staining with Trypan blue. One representative proliferation curve and the mean of pooled data of three biological replicates ($n = 3$) performed in technical triplicates are shown. **b** Proliferation was further determined by flow cytometry using counting beads. Bars represent the mean of three biological replicates ($n = 3$) performed in technical triplicates. **c** Representative flow cytometry plots of BrdU cell cycle analysis and pooled data from three biological replicates ($n = 3$) performed in technical triplicates are shown. Bars represent the mean of % cells in S phase. Student's *t* test was used: * $p < 0.05$, ** $p < 0.01$, *** $p < 0.001$. Error bars indicate SD

DOT1Li induce a durable inhibition of proliferation and favor their response to chemotherapy. Therefore, this observation indicated considerable flexibility regarding dose scheduling of combinations of inhibitors and chemotherapy in clinical translation.

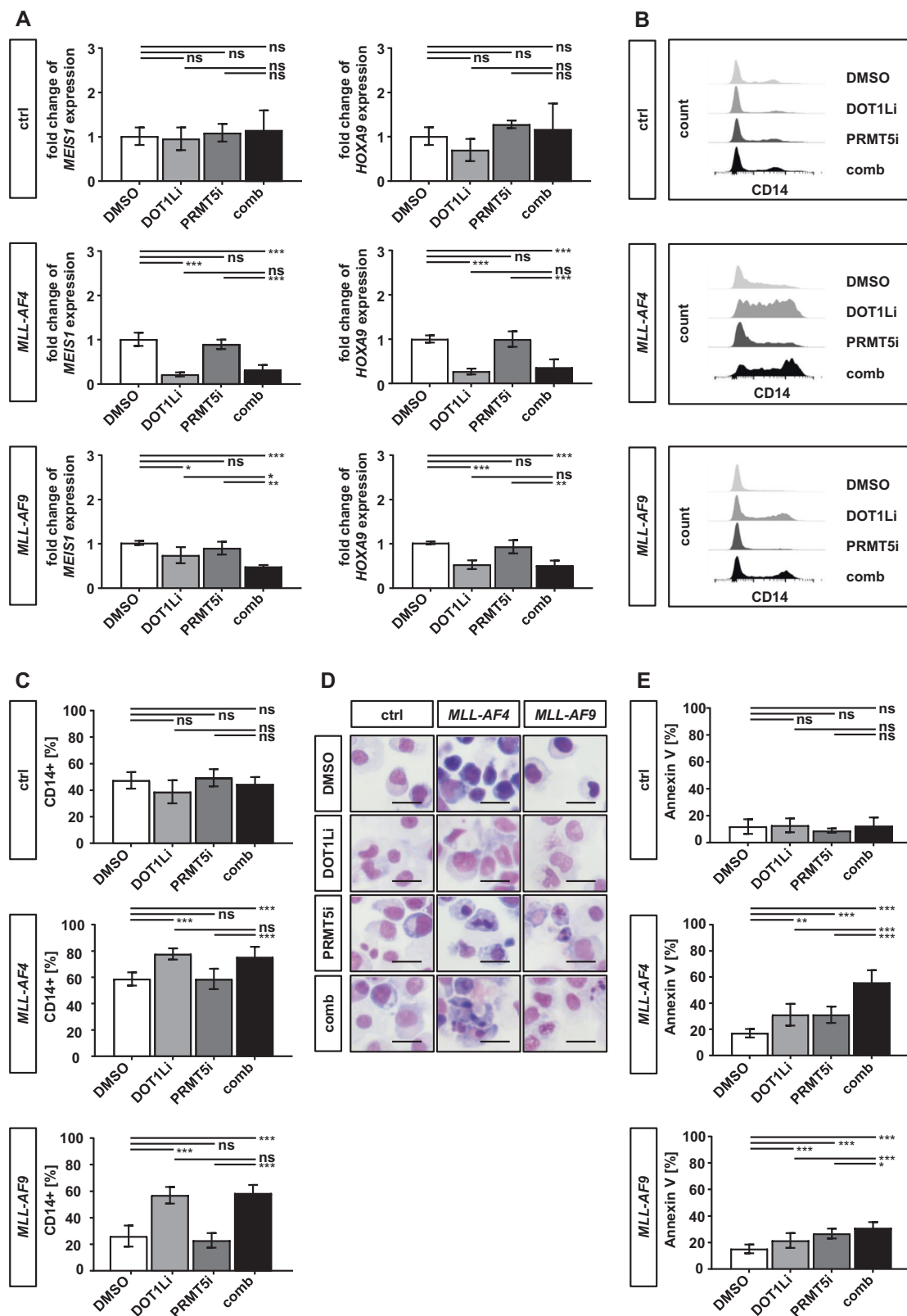
Discussion

In this study we used CRISPR/Cas9 to generate both $t(4;11)$ and $t(9;11)$ chromosomal translocations encoding the *MLL-AF4* or *-AF9* and reciprocal *AF4-* or *AF9-MLL* fusion products in primary human HSPCs to establish an authentic human leukemia model based on patient-specific sequences. CRISPR/Cas9 demonstrated superior effects modifying CD34⁺ huCB to induce balanced translocations than our previously used TALEN technology [11]. The main limitation of our previous study was the long duration until only few polyclonal *MLLr* cells in the beginning reached monoclonal purity for further analysis [11]. By using CRISPR/Cas9 with higher efficiency in primary cells, we were able to generate 100% pure *MLLr* cells within only 30 days. Further advantage to our previous study is the development of not only an *MLL-AF9* but also an accurate human *MLL-AF4* model. Until now no human model exists that recapitulates all features of *MLL-AF4* patient cells although significant efforts have been made leading to the hypothesis that *MLL-AF4* is potentially unable to transform cells without, for example, cooperating mutation partners or the reciprocal fusion product [38–41]. Nevertheless, recently, Lin et al. have developed a human *MLL-AF4* model by using a retroviral transduction approach [42]. Although they successfully recapitulated the lymphoid phenotype of the disease, the study experienced limitations: they used retroviral constructs resulting in unphysiologically high-titer virus to be able to transform human CD34⁺ cells and furthermore, the murine Af4 partner did not mimic the underlying human patient disease. In contrast, our model based on patient-specific sequences with complete

translocation modeling the consequences of endogenous oncogene activation, bypasses these limitations by demonstrating unlimited in vitro growth potential and recapitulating all molecular aspects of the disease demonstrated by high similarity to *MLLr* patient cells detected in RNA-seq. Furthermore, we were able to identify the *MLL* leukemic stem cell signature by expression of high levels of *CBX5*, *MYB*, and *HMGB3* in our *MLLr* cells, another hallmark of *MLLr* leukemias [34, 43]. In addition, under myeloid culture conditions the *MLLr* cells displayed immature morphology and the typical myelomonocytic phenotype with known patient-elevated surface markers like CD9 and CD32 [11, 25]. Thus, our genome engineered human system provides a reliable model to unravel the pathogenesis of *MLLr* leukemogenesis and forms the basis for testing novel therapeutic strategies.

Despite large investment and many new available compounds in drug development, the success rate of translation to the clinic is very low. One major explanation is flawed preclinical research suffering from using the right model that is pivotal to bridge the translational gap [44]. Primary leukemic cells differentiate rapidly in in vitro cultures and mouse models bear problems in the interpretation of the results since there are known differences between the genetic and epigenetic profile of mouse and human. Furthermore, animal models cannot accurately reproduce the disease with all its complexities [45]. Therefore, the selection of a validated and authentic human model is essential to address the clinical questions. By using our patient-like human *MLLr* model with indefinite growth in in vitro cultures we can at least in part overcome these limitations.

Although DOT1Li showed promising results in treating *MLLr* leukemia in preclinical studies, the expected effectiveness to promote long-term remission in *MLLr* patients held off [17]. This reflects the necessity to target *MLLr* leukemia more profoundly than with single treatment. It is known that overexpression of *PRMT5* has critical implications in cancer development providing the rationale for a therapeutic approach to inhibit *PRMT5* methyltransferase activity [46]. Moreover, it has been demonstrated that inhibition of *PRMT5* impaired leukemia development in *MLLr* mouse models and we therefore focused on *PRMT5i* as combination partner of DOT1Li [21, 35, 47]. In our human *MLLr* model, we provided robust data showing that *PRMT5* was overexpressed in our system and subsequently combining two targeted therapies could serve as an effective therapeutic strategy in *MLLr* leukemia: synergistic treatment leads to increased inhibition of proliferation, impairment of cell cycle, differentiation, downregulation of target genes and finally apoptosis of the *MLLr* cells whereas control cells were not affected. Interestingly, DOT1L and *PRMT5* unfold their oncogenic properties in different pathogenic pathways: only DOT1Li was responsible for



downregulation of target genes, hereby unblocking the myeloid differentiation as hallmark of *MLLr* leukemia [48]. This is in line with others suggesting that PRMT5i

compromises an *MLLr* LSC signature and self-renewal by an alternative pathway like transcriptional silencing of CDKN1a or regulated upstream by the PAFc complex

◀ **Fig. 5** Inhibition of DOT1L and PRMT5 compromise *MLL* leukemogenesis by alternative pathways resulting in increased apoptosis of *MLLr* cells. *MLL-AF4-AF9* or culture-expanded CD34⁺ huCB control cells were treated with either 1 μM DOT1Li, 1 μM PRMT5i, in combination or vehicle (DMSO). **a** Target gene expression analyzed by qPCR from three biological replicates ($n = 3$) performed in technical triplicates is shown. Results were normalized on 18S rRNA and control cells were used as calibrator. **b** Representative flow cytometry histograms of CD14 expression as marker of differentiation, and **c** pooled data from three biological replicates ($n = 3$) performed in technical triplicates is shown. **d** Images show representative morphologies of *MLLr* and control cells displaying increased cell differentiation (DOT1Li) and cell death (PRMT5i) after drug treatment. Scale bars define 20 μm. **e** To demonstrate synergistic apoptotic induction, externalization of phosphatidylserine was analyzed by Annexin V staining from three biological replicates ($n = 3$) performed in technical triplicates by flow cytometry. Bars represent the mean. Student's *t* test was used: * $p < 0.05$, ** $p < 0.01$, *** $p < 0.001$. Error bars indicate SD

[21, 35]. In contrast to Serio et al. and our study, Kaushik et al. describe an increased differentiation upon PRMT5i in a *MLLr* mouse model [21, 35]. Although these studies provide important insights, it remains uncertain whether the experimental models accurately reflect the pathology underlying the disease as it manifests in human patients. Thus, this observation stresses the need of human patient-like models in testing pharmacological drugs in the future.

Leukemic patients bearing *MLL*-rearrangements are most commonly treated with cytarabine. Therefore, we combined exposition of *MLLr* cells to cytarabine with DOT1Li and PRMT5i treatment in order to evaluate how these compounds might influence each other with regard to clinical translation. Remarkably, we detected complementary effects in simultaneous and sequential treatment approaches suggesting flexible dose scheduling. This flexibility could result in optimized efficacy of the combined treatment and reduced chemotherapy-associated side effects.

In summary, our study highlights the feasibility of engineering chromosomal translocations at their endogenous loci in primary human cells in high frequency to generate pure *MLLr* cells in a short period of time. Moreover, our genome editing approach overcomes the limitations of previous pharmacological studies and provides the rationale to treat poor prognosis *MLLr* leukemias by combining DOT1L and PRMT5 inhibitors in clinical trials. Further, both compounds may be combined with standard chemotherapy to reverse chemoresistance of *MLLr* cells.

Methods

Genomic engineering via CRISPR/Cas9

Single guide (sg)RNAs were designed with CRISPRscan [49] to target patient-specific *MLL-AF4* and *-AF9*

breakpoints [4, 22, 23]. Possible sgRNAs with high CRISPRscan score resulting in high activity with low off-target activity were selected. sgRNAs comprise T7 promoter, PAM sequence, target complementary region and the scaffold overlapping region. For higher efficiency “ATAGC” sequence was added to the 3' end [50]. Designed oligonucleotides (Supplementary Table 1, Sigma-Aldrich, St. Louis, Missouri, USA) and plasmid PX458 (Addgene, Cambridge, Massachusetts, USA) were used to generate the DNA template (KAPA HiFi HotStart ReadyMix PCR Kit, Wilmington, Massachusetts, USA) following in vitro transcription (NEB Hi-Scribe T7 Kit, Ipswich, Massachusetts, USA, Zymo RNA Clean and concentrate-25, Irvine, California, USA) according to the manufacturer's protocol. Cas9 protein was provided by PNAbio (Newbury Park, California, USA) as purified protein for the formation of the RNP complex (1 μg + 1 μg) accomplished after 15 min of co-incubation at room temperature. Electroporation was performed using the 4D-Nucleofector (Lonza, Basel, Switzerland) according to the manufacturer's protocol for K562 or CD34⁺ cells (Lonza P3 Primary Cell 4D-Nucleofector X Kit S) and as previously described [11]. Cutting efficiencies of respective sgRNAs were determined after isolation of genomic DNA (Macherey Nagel NucleoSpin DNA Rapid Lyse, Dueren, Germany) via site-specific PCR (Supplementary Table 2, Thermo Fisher Scientific AccuPrime Pfx DNA Polymerase, Waltham, Massachusetts, USA) and T7 endonuclease I assay (NEB T7 endonuclease I). Gel images were analyzed with ImageJ [51]. Translocations were induced in CD34⁺ cord blood cells applying *MLL* and *AF4/AF9* sgRNAs in pair (1 μg each) together with Cas9 protein. Rearrangements and reciprocal translocations were identified via PCR of 100 ng genomic DNA (Supplementary Table 3, Thermo Fisher Scientific AccuPrime Pfx DNA Polymerase), Sanger sequencing, fluorescence in situ hybridization (FISH, Cytocell *MLL (KMT2A)* Breakapart Probe, Cambridge, UK) and karyotyping as described previously [11, 52].

RNA sequencing and gene expression analyses

RNA was isolated (Macherey Nagel NucleoSpin RNA Kit) and quality assessment was carried out by NanoDrop (Thermo Fisher Scientific) and Bioanalyzer measurements (Agilent, Santa Clara, California, USA). RNA sequencing (RNA-seq) data quality was assessed using FastQC (V0.11.4, Babraham Institute, Cambridge, UK) [53] to identify sequencing cycles with low average quality, adaptor contamination or repetitive sequences from PCR amplification, before aligning reads with STAR (V2.5.4b) [54] against the Ensembl *H. sapiens* genome V91 allowing gapped alignments to account for splicing. Alignment quality was analyzed using samtools (V1.1) [55].

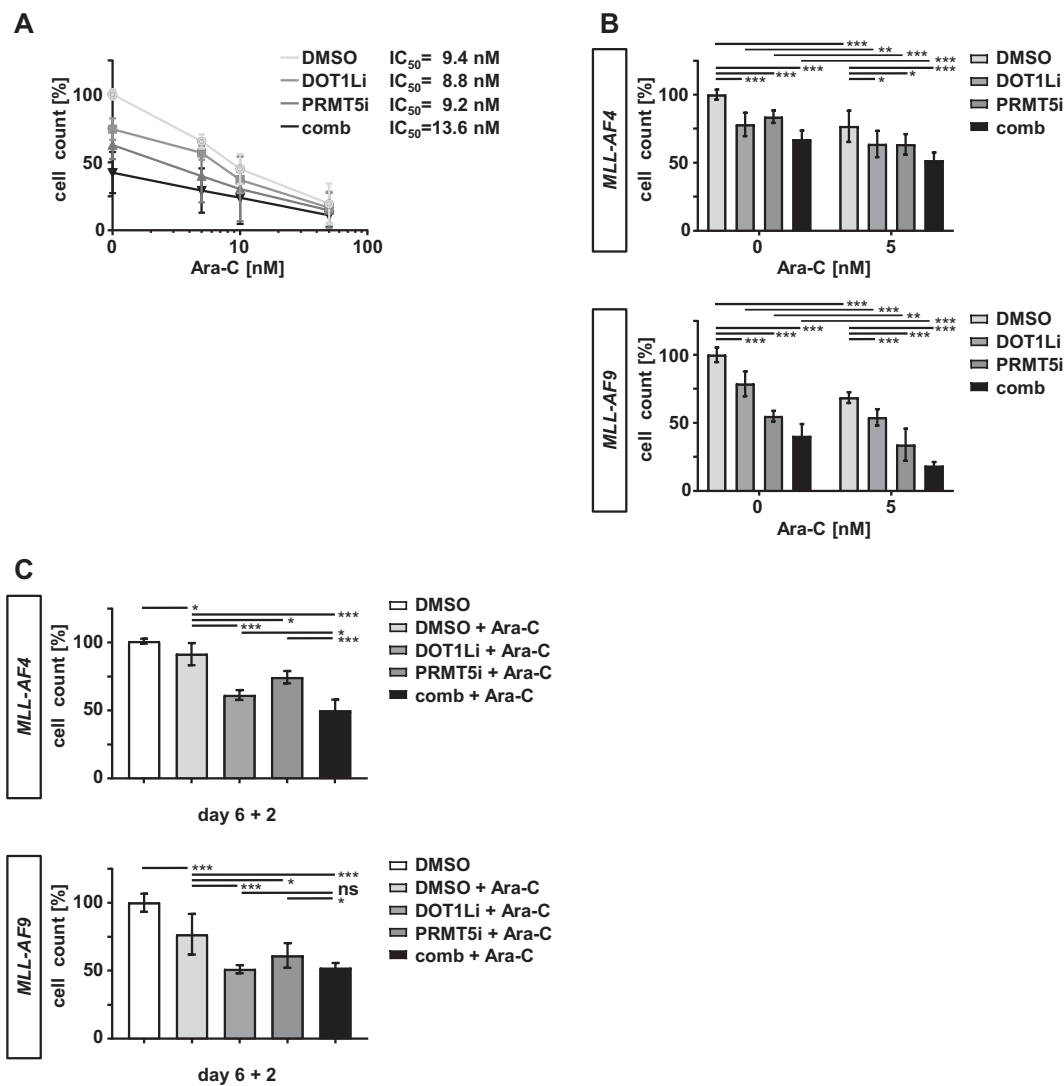


Fig. 6 Treatment with DOT1Li and PRMT5i sensitizes *MLLr* cells to chemotherapy. **a** *MLLr* cells were treated with either 1 μ M DOT1Li, 1 μ M PRMT5i, in combination or vehicle (DMSO) for 6 days and increasing concentrations of Ara-C were co-administered to the culture system. The mean of two biological replicates ($n = 2$) performed in technical triplicates is shown. **b** Ara-C (5 nM) or vehicle (PBS) was used simultaneously with respective inhibitors in proliferation assay for 6 days. The mean of three biological replicates ($n = 3$) performed

in technical triplicates is shown. **c** For sequential analysis, initial treatment for 6 days with respective compounds was washed out and cells were reseeded with vehicle (PBS) or 5 nM Ara-C and monitored for 2 days (6 + 2). The mean of three biological replicates ($n = 3$) performed in technical triplicates is shown. Proliferation was determined by flow cytometry using counting beads. Student's *t* test was used: * $p < 0.05$, ** $p < 0.01$, *** $p < 0.001$. Error bars indicate SD

Normalized read counts for all genes were obtained using GenomicAlignments (V1.14.2) and DESeq2 (V1.18.1) [56]. Transcripts covered with < 50 reads were excluded from subsequent analyses leaving 13 267 genes for determining differential expression. Significance thresholds were set to \log_2 fold-change ≥ 1 and BH-adjusted p -value ≤ 0.01 . Surrogate variable analysis (sva, V3.26.0) was used to minimize unwanted variation between samples [57]. Raw counts from DESeq2 went into calculating nRPKMs (normalized Reads Per Kilobase per Million total reads) as a measure of relative gene expression as motivated before [58]. Gene set enrichments were determined with GSEA (V3.0) [29, 30]

using gene sets provided by Andersson et al. and Stam et al. [27, 28]. RNA-seq data have been deposited in NCBI's Gene Expression Omnibus (GEO) and are accessible through GEO Series accession number GSE128342.

DOT1L and PRMT5 inhibition assays

DOT1L inhibitor EPZ004777 (Tocris, Bristol, UK) or EPZ5676 (Selleck Chemicals LLC, Houston, Texas, USA) and PRMT5 inhibitor EPZ015666 (Sigma-Aldrich) or EPZ015938 (GSK3326595, Selleck Chemicals LLC) were prepared in stock solutions with DMSO.

Cytarabine (Ara-C, Stadapharm, Bad Vilbel, Germany) was diluted in PBS for stock solutions. *MLLr* cells and culture-expanded CD34⁺ huCB control cells seeded with 7.5×10^5 cells/mL were subjected to inhibitor treatment for a total of 6 days in liquid culture. Cells were retreated and reseeded at original density every 2 days. For sequential experiments, cells were preincubated for 6 days, compounds were washed out and cells were reseeded at 7.5×10^5 cells/mL.

BrdU cell-cycle and apoptosis analyses

BrdU incorporation assays were performed using FITC BrdU flow kit (BD Biosciences) according to the manufacturer's protocol with cells pulsed with BrdU for 40 min. Cells were co-stained with 7-AAD for DNA content measurement. Annexin V apoptosis staining was performed using FITC Annexin V Apoptosis Detection Kit I (BD Biosciences) to evaluate early apoptotic cells and accumulated dead cells according to the manufacturer's protocol. All experiments were performed following single cell gating. Analyses were performed using FlowJo (Tree Star).

May-Gruenwald-Giemsa cytospin staining

Cytospins were prepared and stained as previously described [10]. Images were collected using a Nikon Eclipse TS100 microscope with an $\times 40$ objective and a Nikon Digital Sight camera using NIS elements software (Nikon, Tokyo, Japan) at a resolution of 1280×960 pixels.

Statistical analyses

Statistical methods (two-sided Student's *t* test), sample sizes, replicates and *p*-values are presented in each figure legends. Variance was factored into statistical tests where applicable. *P*-value < 0.05 was considered statistically significant. Data were analyzed with Prism 7.03 (GraphPad Software, La Jolla, California, USA). IC₅₀ values of dose response curves were interpolated from a four-parameter logistic model. Synergy was calculated using the Chou-Talalay method [59]. The combination index (CI) was used to define additivity (CI = 1), synergism (CI < 1), and antagonism (CI > 1). CI values: 0–0.1, very strong synergism; 0.1–0.3, strong synergism; 0.3–0.7, synergism; 0.7–0.85, moderate synergism; 0.85–0.90, slight synergism; 0.90–1.10, nearly additive).

Acknowledgements We thank the Flow Cytometry Core Facility Berg of the University Hospital Tuebingen for their excellent technical support. Likewise, we would like to thank the Department of Obstetrics and Gynecology of the University Hospital Tuebingen for providing human cord blood, and the core facility c.ATG of the University Hospital Tuebingen for preparing the RNA-seq libraries,

sequencing the samples and data quality control. Furthermore, we thank Dr. Johan Jeong for his technical support in the analysis of the RNA-seq data. CS was supported by a Junior Research Group Grant of the Interdisciplinary Centre for Clinical Research (IZKF, 2383-0-0), the Wuerttembergischer Krebspreis and the Clinician Scientist Program of the Faculty of Medicine Tuebingen. DS was supported by a Max Eder Junior Research Group Grant from the Deutsche Krebshilfe, a New Investigator Award of the American Society for Blood and Marrow Transplantation (ASBMT), a Junior Research Group Grant of the Interdisciplinary Centre for Clinical Research (IZKF, 2316-0-0) and the Clinician Scientist Program of the Faculty of Medicine Tuebingen. JMSH was supported by a Margarete-von-Wrangell fellowship through the Ministry of Science, Research and the Arts Baden-Wuerttemberg, a Junior Research Group Grant of the Interdisciplinary Centre for Clinical Research (IZKF, 2386-0-0) and, together with TH, received funding from the *decipherPD* transnational consortium on Epigenomics of Complex Diseases (BMBF grant number 01KU1503).

Author contributions KAS and CS designed and performed the research, analyzed data and wrote the paper. HK, SDS, HS, DS, TH, JMSH, BM, and FF performed research and analyzed data. All authors edited the paper for content.

Compliance with ethical standards

Conflict of interest The authors declare that they have no conflict of interest.

Publisher's note: Springer Nature remains neutral with regard to jurisdictional claims in published maps and institutional affiliations.

References

- Slany RK. The molecular biology of mixed lineage leukemia. *Haematologica*. 2009;94:984–93.
- Meyer C, Burmeister T, Groger D, Tsaur G, Fechina L, Renneville A, et al. The MLL recombinome of acute leukemias in 2017. *Leukemia*. 2018;32:273–84.
- Muntean AG, Hess JL. The pathogenesis of mixed-lineage leukemia. *Annu Rev Pathol*. 2012;7:283–301.
- Meyer C, Hofmann J, Burmeister T, Groger D, Park TS, Emerenciano M, et al. The MLL recombinome of acute leukemias in 2013. *Leukemia*. 2013;27:2165–76.
- Wei J, Wunderlich M, Fox C, Alvarez S, Cigudosa JC, Wilhelm JS, et al. Microenvironment determines lineage fate in a human model of MLL-AF9 leukemia. *Cancer Cell*. 2008;13:483–95.
- Barabe F, Kennedy JA, Hope KJ, Dick JE. Modeling the initiation and progression of human acute leukemia in mice. *Science*. 2007;316:600–4.
- Moriya K, Suzuki M, Watanabe Y, Takahashi T, Aoki Y, Uchiyama T, et al. Development of a multi-step leukemogenesis model of MLL-rearranged leukemia using humanized mice. *PLoS ONE*. 2012;7:e37892.
- Chen W, O'Sullivan MG, Hudson W, Kersey J. Modeling human infant MLL leukemia in mice: leukemia from fetal liver differs from that originating in postnatal marrow. *Blood*. 2011;117:3474–5.
- Chen W, Kumar AR, Hudson WA, Li Q, Wu B, Staggs RA, et al. Malignant transformation initiated by MLL-AF9: gene dosage and critical target cells. *Cancer Cell*. 2008;13:432–40.
- Buechele C, Breese EH, Schneidawind D, Lin CH, Jeong J, Duque-Afonso J, et al. MLL leukemia induction by genome editing of human CD34⁺ hematopoietic cells. *Blood*. 2015;126:1683–94.

11. Schneidawind C, Jeong J, Schneidawind D, Kim IS, Duque-Afonso J, Wong SHK, et al. MLL leukemia induction by t(9;11) chromosomal translocation in human hematopoietic stem cells using genome editing. *Blood Adv.* 2018;2:832–45.
12. Torres R, Martin MC, Garcia A, Cigudosa JC, Ramirez JC, Rodriguez-Perales S. Engineering human tumour-associated chromosomal translocations with the RNA-guided CRISPR-Cas9 system. *Nat Commun.* 2014;5:3964.
13. Choi PS, Meyerson M. Targeted genomic rearrangements using CRISPR/Cas technology. *Nat Commun.* 2014;5:3728.
14. Piganeau M, Ghezraoui H, De Cian A, Guittat L, Tomishima M, Perrouault L, et al. Cancer translocations in human cells induced by zinc finger and TALE nucleases. *Genome Res.* 2013;23:1182–93.
15. Reimer J, Knoess S, Labuhn M, Charpentier EM, Göhring G, Schlegelberger B, et al. CRISPR-Cas9-induced t(11;19)/MLL-ENL translocations initiate leukemia in human hematopoietic progenitor cells in vivo. *Haematologica.* 2017;102:1558–66.
16. Okada Y, Feng Q, Lin Y, Jiang Q, Li Y, Coffield VM, et al. hDOT1L links histone methylation to leukemogenesis. *Cell.* 2005;121:167–78.
17. Stein EM, Garcia-Manero G, Rizzieri DA, Tibes R, Berdeja JG, Savona MR, et al. The DOT1L inhibitor pinometostat reduces H3K79 methylation and has modest clinical activity in adult acute leukemia. *Blood.* 2018;131:2661–9.
18. Zhang B, Dong S, Zhu R, Hu C, Hou J, Li Y, et al. Targeting protein arginine methyltransferase 5 inhibits colorectal cancer growth by decreasing arginine methylation of eIF4E and FGFR3. *Oncotarget.* 2015;6:22799–811.
19. Mongiardi MP, Savino M, Bartoli L, Beji S, Nanni S, Scagnoli F, et al. Myc and Omomyc functionally associate with the Protein Arginine Methyltransferase 5 (PRMT5) in glioblastoma cells. *Sci Rep.* 2015;5:15494.
20. Brinkmann KO, Zhao J, Pourdavoud N, Becker T, Hu T, Olthof S, et al. Suppressed decomposition of organometal halide perovskites by impermeable electron-extraction layers in inverted solar cells. *Nat Commun.* 2017;8:13938.
21. Serio J, Ropa J, Chen W, Mysliwski M, Saha N, Chen L, et al. The PAF complex regulation of Prmt5 facilitates the progression and maintenance of MLL fusion leukemia. *Oncogene.* 2018;37:450–60.
22. Langer T, Metzler M, Reinhardt D, Viehmann S, Borkhardt A, Reichel M, et al. Analysis of t(9;11) chromosomal breakpoint sequences in childhood acute leukemia: almost identical MLL breakpoints in therapy-related AML after treatment without etoposides. *Genes, Chromosomes Cancer.* 2003;36:393–401.
23. Reichel M, Gillert E, Angermuller S, Hensel JP, Heidel F, Lode M, et al. Biased distribution of chromosomal breakpoints involving the MLL gene in infants versus children and adults with t(4;11) ALL. *Oncogene.* 2001;20:2900–7.
24. Breese EH, Dawson C, Buechele C, Breese MR, Cleary ML, Porteus MH. Using genome engineering to prospectively investigate the pathogenesis of MLL translocations in infant acute lymphoblastic leukemia. *Blood.* 2013;122:3722.
25. Aoki Y, Watanabe T, Saito Y, Kuroki Y, Hijikata A, Takagi M, et al. Identification of CD34+ and CD34– leukemia-initiating cells in MLL-rearranged human acute lymphoblastic leukemia. *Blood.* 2015;125:967–80.
26. Baer MR, Stewart CC, Lawrence D, Arthur DC, Mrozek K, Strout MP, et al. Acute myeloid leukemia with 11q23 translocations: myelomonocytic immunophenotype by multiparameter flow cytometry. *Leukemia.* 1998;12:317–25.
27. Andersson AK, Ma J, Wang J, Chen X, Gedman AL, Dang J, et al. The landscape of somatic mutations in infant MLL-rearranged acute lymphoblastic leukemias. *Nat Genet.* 2015;47:330–7.
28. Stam RW, Schneider P, Hagelstein JA, van der Linden MH, Stumpel DJ, de Menezes RX, et al. Gene expression profiling-based dissection of MLL translocated and MLL germline acute lymphoblastic leukemia in infants. *Blood.* 2010;115:2835–44.
29. Subramanian A, Tamayo P, Mootha VK, Mukherjee S, Ebert BL, Gillette MA, et al. Gene set enrichment analysis: a knowledge-based approach for interpreting genome-wide expression profiles. *Proc Natl Acad Sci USA.* 2005;102:15545–50.
30. Mootha VK, Lindgren CM, Eriksson KF, Subramanian A, Sihag S, Lehar J, et al. PGC-1 α -responsive genes involved in oxidative phosphorylation are coordinately downregulated in human diabetes. *Nat Genet.* 2003;34:267–73.
31. Armstrong SA, Staunton JE, Silverman LB, Pieters R, den Boer ML, Minden MD, et al. MLL translocations specify a distinct gene expression profile that distinguishes a unique leukemia. *Nat Genet.* 2002;30:41–47.
32. Lavalley VP, Baccelli I, Kros J, Wilhelm B, Barabe F, Gendron P, et al. The transcriptomic landscape and directed chemical interrogation of MLL-rearranged acute myeloid leukemias. *Nat Genet.* 2015;47:1030–7.
33. Mullighan CG, Kennedy A, Zhou X, Radtke I, Phillips LA, Shurtleff SA, et al. Pediatric acute myeloid leukemia with NPM1 mutations is characterized by a gene expression profile with dysregulated HOX gene expression distinct from MLL-rearranged leukemias. *Leukemia.* 2007;21:2000–9.
34. Somervaille TC, Matheny CJ, Spencer GJ, Iwasaki M, Rinn JL, Witten DM, et al. Hierarchical maintenance of MLL myeloid leukemia stem cells employs a transcriptional program shared with embryonic rather than adult stem cells. *Cell Stem Cell.* 2009;4:129–40.
35. Kaushik S, Liu F, Veazey KJ, Gao G, Das P, Neves LF, et al. Genetic deletion or small-molecule inhibition of the arginine methyltransferase PRMT5 exhibit anti-tumoral activity in mouse models of MLL-rearranged AML. *Leukemia.* 2018;32:499–509.
36. Daigle SR, Olhava EJ, Therkelsen CA, Basavapathruni A, Jin L, Boriack-Sjodin PA, et al. Potent inhibition of DOT1L as treatment of MLL-fusion leukemia. *Blood.* 2013;122:1017–25.
37. Jansson M, Durant ST, Cho EC, Sheahan S, Edelmann M, Kessler B, et al. Arginine methylation regulates the p53 response. *Nat Cell Biol.* 2008;10:1431–9.
38. Bueno C, Montes R, Melen GJ, Ramos-Mejia V, Real PJ, Ayllon V, et al. A human ESC model for MLL-AF4 leukemic fusion gene reveals an impaired early hematopoietic-endothelial specification. *Cell Res.* 2012;22:986–1002.
39. Bursen A, Schwabe K, Ruster B, Henschler R, Ruthardt M, Dingermann T, et al. The AF4.MLL fusion protein is capable of inducing ALL in mice without requirement of MLL.AF4. *Blood.* 2010;115:3570–9.
40. Krivtsov AV, Feng Z, Lemieux ME, Faber J, Vempati S, Sinha AU, et al. H3K79 methylation profiles define murine and human MLL-AF4 leukemias. *Cancer Cell.* 2008;14:355–68.
41. Montes R, Ayllon V, Gutierrez-Aranda I, Prat I, Hernandez-Lamas MC, Ponce L, et al. Enforced expression of MLL-AF4 fusion in cord blood CD34+ cells enhances the hematopoietic repopulating cell function and clonogenic potential but is not sufficient to initiate leukemia. *Blood.* 2011;117:4746–58.
42. Lin S, Luo RT, Ptasińska A, Kerry J, Assi SA, Wunderlich M, et al. Instructive role of MLL-fusion proteins revealed by a model of t(4;11) pro-B Acute Lymphoblastic Leukemia. *Cancer Cell.* 2016;30:737–49.
43. Somervaille TC, Cleary ML. Identification and characterization of leukemia stem cells in murine MLL-AF9 acute myeloid leukemia. *Cancer Cell.* 2006;10:257–68.

44. Kerbel RS. Human tumor xenografts as predictive preclinical models for anticancer drug activity in humans: better than commonly perceived-but they can be improved. *Cancer Biol Ther.* 2003;2(4 Suppl 1):S134–139.
45. Bouchlaka MN, Sckisel GD, Chen M, Mirsoian A, Zamora AE, Maverakis E, et al. Aging predisposes to acute inflammatory induced pathology after tumor immunotherapy. *J Exp Med.* 2013;210:2223–37.
46. Yang Y, Bedford MT. Protein arginine methyltransferases and cancer. *Nat Rev Cancer.* 2013;13:37–50.
47. Shi J, Wang E, Milazzo JP, Wang Z, Kinney JB, Vakoc CR. Discovery of cancer drug targets by CRISPR-Cas9 screening of protein domains. *Nat Biotechnol.* 2015;33:661–7.
48. Daigle SR, Olhava EJ, Therkelsen CA, Majer CR, Sneeringer CJ, Song J, et al. Selective killing of mixed lineage leukemia cells by a potent small-molecule DOT1L inhibitor. *Cancer Cell.* 2011;20:53–65.
49. Moreno-Mateos MA, Vejnar CE, Beaudoin JD, Fernandez JP, Mis EK, Khokha MK, et al. CRISPRscan: designing highly efficient sgRNAs for CRISPR-Cas9 targeting in vivo. *Nat Methods.* 2015;12:982–8.
50. Gundry MC, Brunetti L, Lin A, Mayle AE, Kitano A, Wagner D, et al. Highly efficient genome editing of murine and human hematopoietic progenitor cells by CRISPR/Cas9. *Cell Rep.* 2016;17:1453–61.
51. Schneider CA, Rasband WS, Eliceiri KW. NIH Image to ImageJ: 25 years of image analysis. *Nat Methods.* 2012;9:671–5.
52. Breese EH, Buechele C, Dawson C, Cleary ML, Porteus MH. Use of genome engineering to create patient specific *MLL* translocations in primary human hematopoietic stem and progenitor cells. *PLoS ONE.* 2015;10:e0136644.
53. Andrews S. FastQC: a quality control tool for high throughput sequence data. 2010. <http://www.bioinformatics.babraham.ac.uk/projects/fastqc>
54. Dobin A, Davis CA, Schlesinger F, Drenkow J, Zaleski C, Jha S, et al. STAR: ultrafast universal RNA-seq aligner. *Bioinformatics.* 2013;29:15–21.
55. Li H, Handsaker B, Wysoker A, Fennell T, Ruan J, Homer N, et al. The sequence alignment/map format and SAMtools. *Bioinformatics.* 2009;25:2078–9.
56. Love MI, Huber W, Anders S. Moderated estimation of fold change and dispersion for RNA-seq data with DESeq2. *Genome Biol.* 2014;15:550.
57. Leek JT, Johnson WE, Parker HS, Jaffe AE, Storey JD. The sva package for removing batch effects and other unwanted variation in high-throughput experiments. *Bioinformatics.* 2012;28:882–3.
58. Srinivasan K, Friedman BA, Larson JL, Lauffer BE, Goldstein LD, Appling LL, et al. Untangling the brain's neuroinflammatory and neurodegenerative transcriptional responses. *Nat Commun.* 2016;7:11295.
59. Chou TC. Theoretical basis, experimental design, and computerized simulation of synergism and antagonism in drug combination studies. *Pharm Rev.* 2006;58:621–81.